### Title

Imaging of the region of the osteochondral junction (OCJ) using a 3D adiabatic inversion recovery prepared ultrashort echo time cones (3D IR-UTE-cones) sequence at 3 T




### Journal

NMR in Biomedicine, 32(5)

### ISSN

0952-3480



### Authors

Ma, Ya-Jun
Jerban, Saeed
Carl, Michael
et al.



### Publication Date

2019-05-01

### DOI

10.1002/nbm.4080

Peer reviewed

Received: 23 October 2018 | Revised: 16 January 2019 | Accepted: 18 January 2019

DOI: 10.1002/nbm.4080

RESEARCH ARTICLE

WILEY NMR IN BIOMEDICINE

# Imaging of the region of the osteochondral junction (OCJ) using a 3D adiabatic inversion recovery prepared ultrashort echo time cones (3D IR-UTE-cones) sequence at 3 T

Ya-Jun Ma[1] | Saeed Jerban[1] | Michael Carl[2] | Lidi Wan[1] | Tan Guo[1] | Hyungseok Jang[1] | Graeme M. Bydder[1] | Eric Y. Chang[1,3] | Jiang Du[1]

[1] Department of Radiology, University of California, San Diego, CA, USA

[2] GE Healthcare, San Diego, CA, USA

[3] Radiology Service, VA San Diego Healthcare System, San Diego, CA, USA

**Correspondence**
Jiang Du, PhD, University of California, San Diego, Department of Radiology, San Diego, CA 92103-8226, USA.
Email: jiangdu@ucsd.edu

**Funding information**
NIH, Grant/Award Numbers: 1R01 AR062581, 1R01 NS092650 and 1R01 AR068987; VA Clinical Science and Rehabilitation Research & Development Services, Grant/Award Numbers: 1I01CX001388 and I01RX002604

The purpose of this study is to develop a 3D adiabatic inversion recovery prepared ultrashort echo time Cones (3D IR-UTE-Cones) sequence for high resolution and contrast imaging of the region of osteochondral junction (OCJ) of human knee joint using a clinical 3 T scanner. A feasibility study on direct imaging of the OCJ region was performed on a human patellar cartilage sample and on eight cadaveric knee joints using $T_1$-weighted, proton density (PD)-weighted and short-$T_2$-weighted 3D IR-UTE-Cones sequences. Contrast to noise ratio was measured to evaluate the effectiveness of the 3D IR-UTE-Cones sequences for selective imaging of the OCJ region. Computed tomography imaging was performed in parallel for the cadaveric knee joints. The optimized $T_1$-weighted 3D IR-UTE-Cones sequence was used to image the knee joints of eight healthy volunteers and six patients with osteoarthritis (OA) to evaluate morphological changes in the OCJ region. Clinical PD- and $T_2$-weighted FSE sequences were also performed for comparison. The $T_1$-weighted 3D IR-UTE-Cones sequence showed high resolution and contrast bright band of the normal OCJ region in the cadaveric joints. Normal OCJ appearances were also seen in healthy volunteers. Abnormal OCJ regions, manifested as ill-defined, focal loss or non-visualization of the high intensity band adjacent to the subchondral bone plate, were observed in the knee joints of both ex vivo and in vivo OA patients. The 3D IR-UTE-Cones sequence can image OCJ regions ex vivo and in vivo, with abnormalities depicted with high resolution and contrast. The technique may be useful for demonstrating involvement of OCJ regions in early OA.

**KEYWORDS**

3D ultrashort echo time, adiabatic inversion recovery, calcified cartilage, osteochondral junction

## 1 | INTRODUCTION

Osteoarthritis (OA) affects at least 30 million adults in the United States and has a substantial impact on the country's healthcare system, with a total annual cost estimated at $5700 per patient.[1] OA is considered a whole joint disease, with pathologic changes that often involve all of the

**Abbreviations used:** 3D IR-UTE-Cones, 3D adiabatic inversion recovery prepared ultrashort echo time Cones; AFI-VFA, actual flip angle imaging and variable flip angle; BW, receiver bandwidth; CNR, contrast to noise ratio; CT, computed tomography; DIR, dual adiabatic inversion recovery; FOV, field of view; FS, fat saturation; IR, inversion recovery; OA, osteoarthritis; OCJ, osteochondral junction; PD, proton density; SNR, signal to noise ratio; UTE, ultrashort echo time; μCT, micro-computed tomography

  

constituent joint tissues.[2] Of increasing interest is the region of the osteochondral junction (OCJ), which encompasses the tissues between the deep uncalcified layers of cartilage and the marrow spaces of the trabecular bone. It includes the deep radial uncalcified cartilage, tidemark, calcified cartilage and subchondral bone plate.[3] In the strictest sense, the OCJ is the region where calcified cartilage meets subchondral bone. However, by analogy to the enthesis, which is the region where tendons or ligaments meet bone, it is useful to consider the tissues between the superficial layers of articular cartilage and the subchondral bone marrow as a whole group, which, like the enthesis, is concerned with the dissipation of stress in a region between semirigid and rigid tissues. While these tissues are avascular in the normal joint, in OA, osteoclasts are activated and form channels through the subchondral bone plate, which allow blood vessels and nerves to extend from the marrow into deep cartilage.[4,5] This is associated with a cascade of abnormalities, including local inflammation and upregulation of metalloproteinase activity, extracellular matrix degradation, reduction of cartilage load-bearing capacity and degenerative change.[3,4,6] These changes may be relevant in the pathogenesis of OA.

MRI is widely used to directly and non-invasively evaluate articular cartilage, and plays an important role in the clinical diagnosis and treatment of OA.[7,8] MRI of the OCJ region is difficult though, due to the short mean transverse relaxation times (ie short $T_2$ or $T_2^*$) of deep radial uncalcified articular cartilage, calcified cartilage and subchondral bone, which results in little or no signal when conventional pulse sequences are used.[9] Ultrashort echo time (UTE) sequences have been employed to overcome this limitation,[10] and have been used to evaluate the OCJ region. Studies have focused on 2D acquisition techniques,[9-14] and high contrast images of the OCJ region have been achieved by combining UTE acquisitions with long $T_2$ signal suppression schemes including dual echo acquisition and echo subtraction, single adiabatic inversion recovery (IR) and dual adiabatic inversion recovery (DIR) pulses.[9-14] These techniques can effectively suppress signals from the more superficial layers of uncalcified cartilage (eg the superficial, middle and upper deep layers), which have longer $T_2$ and $T_2^*$ values, as well as marrow fat, leaving the OCJ to be selectively imaged. However, 2D UTE sequences are sensitive to eddy currents, and it is difficult to image the whole knee joint due to strong out-of-slice signal excitation, especially for off-center slices.[15] As a result, there has been relatively little clinical work published using 2D UTE imaging techniques to evaluate the OCJ region.

Compared with 2D UTE sequences, 3D UTE sequences have the advantage of reducing through-plane partial volume effects, which is important for imaging the thin (ie 100–200 μm) and curved OCJ region.[16] Multi-echo 3D UTE techniques with echo subtraction or $T_2^*$ fitting have been used for this purpose, but there have been problems with low OCJ region contrast and the need for intensive post-processing.[17-19] For clinical purposes, an optimal 3D UTE sequence should provide whole joint coverage, show the OCJ region with high contrast, be obtainable in clinically acceptable scan time and require little or no post-processing.

The purpose of this study was to develop 3D adiabatic IR prepared UTE Cones (3D IR-UTE-Cones) sequences for volumetric imaging of the OCJ region with high spatial resolution and contrast in clinically acceptable scan times. A patellar sample was used to demonstrate the feasibility of OCJ region imaging with the 3D IR-UTE-Cones sequence. Following this, eight cadaveric human knee joints were used to optimize the sequence parameters for high contrast imaging of the OCJ region in clinical feasible scan times. Finally, the 3D IR-UTE-Cones sequence was used in eight healthy volunteers and six patients with OA to assess the clinical feasibility of imaging the OCJ region in vivo.

## 2 | MATERIALS AND METHODS

### 2.1 | Specimens

A patellar sample was harvested from a normal knee joint (male, 31 years old). A transverse slab of about 8 mm thickness was cut and stored in phosphate buffered saline soaked gauze at 4°C prior to MR and micro-computed tomography (μCT) imaging. Eight cadaveric human knee joints were obtained from eight donors (six males and two females, age range 27–96 years old, mean ± standard deviation of 66 ± 28 years) from tissue banks approved by our Institutional Review Board. The specimens were stored frozen at −80°C for about two months, and then taken out to thaw at room temperature for 36 h before MRI.

### 2.2 | In vivo subjects

Two groups of human subjects were included in this study. The first group consisted of eight healthy volunteers with a mean ± standard deviation age of 37 ± 13 years (four males and four females). The second group consisted of six OA patients with mean ± standard deviation age of 58 ± 14 years (two males and four females). The OA patients were diagnosed based on plain radiography before MR experiments. Informed consent was obtained from all subjects in accordance with our institutional review board guidelines before MRI.

### 2.3 | Pulse sequence

The 3D IR-UTE-Cones pulse sequence was implemented on a 3 T MR750 scanner (GE Healthcare Technologies, Milwaukee, WI, USA). The sequence combined a basic 3D UTE-Cones sequence with an adiabatic IR preparation pulse (duration 6 ms).[20] To improve the acquisition

efficiency, a series of spokes ($N_{sp}$) was acquired after each IR pulse (Figure 1A). Fat signal was suppressed with a conventional chemical shift fat saturation (FS) module before the acquisition spoke trains. The time interval between two adjacent spokes was defined as $\tau$. For each spoke, a short rectangular pulse (eg 50 μs) was used for non-selective signal excitation (Figure 1B), and this was followed by a spiral trajectory data acquisition with conical view ordering (Figure 1C). Data sampling began from the center of *k*-space and continued outwards. It was begun as soon as was practical after the RF excitation, with a minimal nominal delay time of 32 μs. Both RF and gradient spoiling were used to crush the residual transverse magnetizations. An eight-channel transmit/receive knee coil was used for both ex vivo and in vivo whole knee joint imaging.

## 2.4 | Contrast mechanism

Figure 2A depicts the regions of different cartilage layers (ie superficial, middle, deep and calcified layers), subchondral bone and marrow fat in the patellar cartilage. Figure 2B illustrates the contrast mechanism for imaging of the OCJ region using the 3D IR-UTE-Cones sequence. Initially, the magnetizations of the more superficial (uncalcified) layers of articular cartilage including the superficial, middle and deep layers are inverted by the adiabatic IR pulse. After this the inverted magnetizations of these layers recover at rates based on their $T_1$ relaxation mechanisms. Since uncalcified cartilage $T_1$ values decrease from the superficial to deep layers,[21] the longitudinal magnetization in the deeper zone recovers faster than those

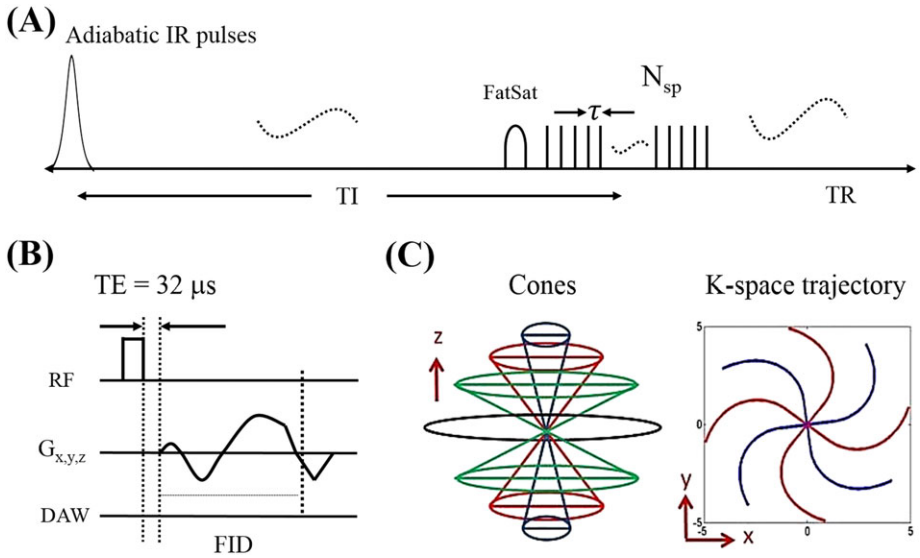


**FIGURE 1** The 3D IR-UTE-cones sequence. This employs an adiabatic inversion pulse for selective signal suppression, followed by 3D UTE-cones data acquisition (a). In the basic 3D UTE-cones sequence a short rectangular pulse is used for signal excitation and this is followed by 3D spiral sampling with a minimal nominal $T_E$ of 32 μs (B). The spiral trajectories are arranged with conical view ordering (C). To speed up data acquisition, multiple spokes can be sampled after each long $T_2$ preparation (a). An FS module is also used in front of the data acquisition spokes

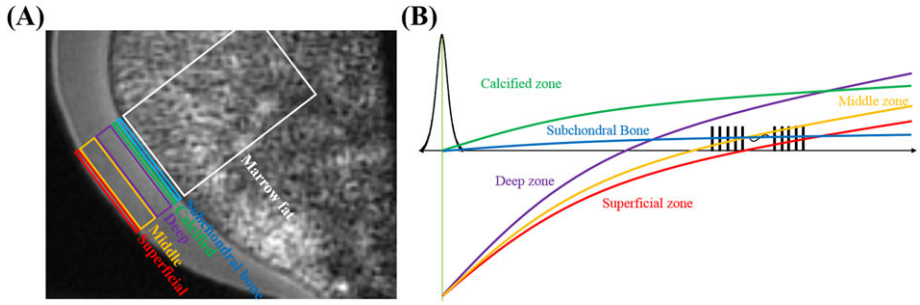


**FIGURE 2** The contrast mechanism for the OCJ region imaging using the 3D IR-UTE-cones sequence. A, the regions of different cartilage layers (ie superficial, middle, deep and calcified layers), subchondral bone and marrow fat in a patellar cartilage. B, the magnetizations of superficial, middle and deep layer uncalcified cartilage are inverted by the adiabatic IR pulse, while calcified layer cartilage and subchondral bone magnetizations are mostly saturated due to their short $T_2$ values. Thus, both the calcified layer cartilage and subchondral bone longitudinal magnetizations recover rapidly from zero after saturation. When $T_I$ is selected to suppress superficial zone cartilage, the calcified layers express a higher signal than the more superficial layer cartilages. Subchondral bone remains low signal due to its low PD

in the middle and superficial layers. As a result, the signal intensity is higher for deep uncalcified cartilage when 3D UTE data acquisitions start near the signal nulling point for the superficial layer cartilage. Tissues of the OCJ region have very short $T_2$ components (much shorter than the duration of the adiabatic IR pulse), and their magnetizations are not inverted by the adiabatic IR pulse and are largely saturated.[22] In addition, the OCJ region tissues have shorter $T_1$ values than the more superficial uncalcified layers of cartilage. As a result, the saturated magnetizations of tissues of the OCJ region recover faster than those of the superficial layers of articular cartilage. This leads to high signal intensity and high contrast for tissues of the OCJ region when the inversion time is close to the nulling point of the superficial layers of articular cartilage.

## 2.5 | Feasibility study on a patellar sample

The feasibility of OCJ region imaging with the 3D IR-UTE-Cones sequence was assessed on a patellar sample from a 31-year-old male donor. To obtain high spatial resolution and signal to noise ratio (SNR) images of the sample, a small birdcage coil which fits in a 30 mL syringe was used for both RF transmission and reception. First, the $T_1$ variation in different cartilage layers and subchondral bone was investigated. A recently reported 3D UTE-Cones actual flip angle imaging and variable flip angle (3D UTE-Cones AFI-VFA) sequence was used to measure the $T_1$ of tissues in the patellar cartilage sample.[23,24] The sequence parameters are listed in Table 1. Then, three additional UTE protocols were evaluated for $T_1$-weighted, proton density (PD)-weighted and selective short $T_2$ imaging of the OCJ region. The $T_1$-weighted 3D IR-UTE-Cones sequence was used to highlight the deep radial and calcified cartilage by selecting a $T_I$ to invert and suppress signals from the more superficial layers of articular cartilage. PD-weighted images were generated with the same IR-UTE-Cones sequence but with a much longer $T_I$. Selective short $T_2$ imaging was performed with a short $T_R$ and short $T_I$ so that very short $T_2$ signals were highlighted, with nearly complete suppression of longer $T_2$ signals.[20] The IR-UTE-Cones sequence parameters were the following. (1) $T_1$ weighted: field of view (FOV) = 6 × 6 × 3 $cm^3$, acquisition matrix = 384 × 384 × 100, voxel size = 156 × 156 × 300 $\mu m^3$, receiver bandwidth (BW) = 125 kHz, $T_R/T_I$ = 1200/450 ms, flip angle = 10°, $N_{sp}$ = 17, $\tau$ = 8.3 ms and total scan time = 1 h 11 min. (2) PD weighted: same parameters as (1) except a longer $T_I$ = 1000 ms. (3) Selective short $T_2$ imaging: FOV = 6 × 6 × 2.4 $cm^3$, acquisition matrix = 256 × 256 × 40, voxel size = 234 × 234 × 600 $\mu m^3$, BW = 125 kHz, $T_R/T_I$ = 133/58 ms, flip angle = 20°, $N_{sp}$ = 5, $\tau$ = 8.3 ms, $n_{ex}$ = 2 and total scan time = 1 h 16 min. For comparison, μCT was also performed with 18 × 18 × 18 $\mu m^3$ resolution. To measure $T_2^*$ of both calcified cartilage and subchondral bone, the same short $T_2$ selective imaging sequence was used but with four longer $T_E$ values (ie 0.2, 0.4, 0.8 and 2.2 ms).

## 2.6 | Ex vivo study of knee joint specimens

The observed OCJ contrast strongly depends on the combination of $T_R$ and $T_I$. To optimize OCJ contrast, the ex vivo knee joint specimens were scanned with the 3D IR-UTE-Cones sequence using a series of $T_I$ values. The sequence parameters were $T_R$ = 1200 ms, $T_I$ = 220, 260, 300, 340, 380, 420, 460, 500, 540, 560, 580, 600, 650, 700 and 800 ms, flip angle = 10°, FOV = 13 × 13 × 8.4 $cm^3$, acquisition matrix = 256 × 256 × 28, voxel size = 508 × 508 × 3000 $\mu m^3$, BW = 250 kHz, $N_{sp}$ = 15, $\tau$ = 6 ms and scan time for each $T_I$ = 9 min 8 s. The $T_I$ values with a higher contrast to noise ratio (CNR) between the OCJ region and superficial cartilage, and between the OCJ region and marrow fat, were used.

**TABLE 1** Sequence parameters for patellar cartilage sample, ex vivo knee joint specimen and in vivo knee joint studies

| 3D UTE-cones AFI (patellar cartilage sample) | 3D IR-UTE-cones (ex vivo knee joint) | 3D IR-UTE-cones (in vivo knee joint) |
|---|---|---|
| FOV = 6 × 6 × 4 $cm^3$,<br>Matrix = 360 × 360 × 100,<br>Voxel size = 167 × 167 × 400 $\mu m^3$,<br>$T_{R1}/T_{R2}$ = 20/100 ms,<br>Flip angle = 45°, BW = 125 kHz,<br>Scan time = 1 h 32 min | FOV = 13 × 13 × 8 $cm^3$,<br>Matrix = 256 × 256 × 40,<br>Voxel size = 508 × 508 × 2000 $\mu m^3$,<br>$T_R/T_I$ = 1200/540 ms,<br>Flip angle = 10°, $N_{sp}$ = 9, $\tau$ = 9 ms,<br>BW = 250 kHz,<br>Oversample factor = 1.2,<br>Scan time = 56 min | FOV = 13 × 13 × 8 $cm^3$,<br>Matrix = 256 × 256 × 40,<br>Voxel size = 508 × 508 × 2000 $\mu m^3$,<br>$T_R/T_I$ = 1200/600 ms,<br>Flip angle = 10°, $N_{sp}$ = 21,<br>$\tau$ = 5.2 ms, BW = 166 kHz,<br>Scan time = 10 min |
| **3D UTE-cones VFA (patellar cartilage sample)** | **Clinical PD-weighted FSE (ex and in vivo knee joint)** | **Clinical $T_2$-weighted FSE (ex and in vivo knee joint)** |
| FOV = 6 × 6 × 4 $cm^3$,<br>Matrix = 360 × 360 × 100,<br>Voxel size = 167 × 167 × 400 $\mu m^3$,<br>$T_R$ = 20 ms, flip angle = 2°, 4°, 6°,<br>8°, 10°, 15°, 20°, 25°, 30°, 35°,<br>BW = 125 kHz,<br>Total scan time = 5 h 13 min | FOV = 15 × 15 $cm^2$,<br>Matrix = 352 × 256,<br>Pixel size = 426 × 586 $\mu m^2$,<br>$T_R$ = 3220 ms, $T_E$ = 27.8 ms,<br>Number of slices = 40,<br>Acceleration factor = 2,<br>Scan time = 2 min 30 s | FOV = 15 × 15 $cm^2$,<br>Matrix = 352 × 256,<br>Pixel size = 426 × 586 $\mu m^2$,<br>$T_R$ = 7585 ms, $T_E$ = 71.5 ms,<br>Number of slices = 40,<br>Acceleration factor = 2,<br>Scan time = 2 min 32 s |

A high resolution and high SNR IR-UTE-Cones sequence was used to image the OCJ region in all the cadaveric knee specimens. Its sequence parameters are listed in Table 1 and the total scan time was 56 min. To facilitate translational imaging of the OCJ in vivo, a faster protocol with a clinically acceptable scan time (ie 10 min) was developed. Most of the sequence parameters were the same except for a higher $N_{sp}$ of 21, a smaller $\tau$ of 5.2 ms and no oversampling. In addition, both clinical PD- and $T_2$-weighted FSE sequences were used for comparison (sequence parameters shown in Table 1). Clinical CT scans were also performed.

## 2.7 | In vivo study of healthy volunteers and patients with OA

Since in vivo cartilage $T_1$ values at body temperature are typically longer than the $T_1$ values of cartilage specimens examined at room temperature, higher $T_I$ values of 500, 550, 600, 650 and 700 ms were tested on one healthy volunteer (male, 28 years old) to determine parameters for optimizing the OCJ region contrast. The optimal $T_I$ was used for subsequent imaging of the OCJ region in healthy volunteers and patients with OA. Other sequence parameters are shown in Table 1. Clinical PD- and $T_2$-weighted FSE sequences were performed for comparison, with parameters the same as for the ex vivo knee joint study.

## 2.8 | Image analysis

The mean signal intensity inside a user drawn region of interest (ROI) within the OCJ region was used for signal calculation, with noise being calculated as the standard deviation of the signal in the ROI placed in an artifact free image background. The CNRs between tissues of the OCJ region and the superficial cartilage ($CNR_{OCJ\_SC}$) and marrow fat ($CNR_{OCJ\_MF}$) were calculated as the respective signal differences divided by the background noise. $T_1$ and $T_2^*$ were also measured using previously reported methods.[21,23,24] Rigid body registration was performed between μCT and UTE images for the patellar sample study. The image co-registration was performed on a 2D basis via the following steps: (1) the corresponding slices of the patella from the $T_1$-weighted IR-UTE-Cones and μCT datasets were selected, (2) a set of four identical points was manually selected on the outer contour of the patella (surface of the cartilage and cut edges of the trabecular bone) on both μCT and MRI images, (3) affine registration transform (linear mapping) was used to perform image registration by matching the four selected control points in the μCT and MRI images employing the Image Processing Toolbox in the MATLAB software and (4) the obtained transformation matrix was used to register μCT and all IR-UTE-Cones images. All analysis algorithms were written in MATLAB. The mean intensity within each of the ROIs was used for subsequent curve fitting.

# 3 | RESULTS

Figure 3 shows high resolution 3D UTE-Cones images, which clearly depict all the components of the patellar cartilage, including the superficial, middle and deep uncalcified layers, calcified cartilage and subchondral bone plate (dark band beneath the calcified cartilage and above the marrow fat). The fitting curves and corresponding $T_1$ values of different regions of cartilage and subchondral bone are also shown. As expected, the $T_1$ values of uncalcified cartilage decrease from the superficial layer (963 ± 23 ms) to the middle layer (937 ± 14 ms) and then the deep layer (741 ± 12 ms). The calcified cartilage has a much lower $T_1$ of 405 ± 16 ms, and the subchondral bone plate has an even shorter $T_1$ of 285 ± 12 ms. The significantly lower $T_1$ values of the calcified cartilage make it possible to highlight the OCJ region with an IR sequence with an appropriate $T_I$. In addition, the $T_2^*$ values of the calcified cartilage and subchondral bone plate in the short $T_2$ IR-UTE-Cones imaging were measured. Both tissues have extremely short $T_2^*$ values (0.42 ± 0.01 ms and 0.31 ± 0.03 ms respectively, Supplementary Figure 1).

Figure 4 shows a comparison between UTE MRI and μCT images of the same patellar cartilage sample. UTE $T_1$-weighted, PD-weighted and short $T_2$ images of the specimen are shown. ROIs including the high intensity band shown with the $T_1$-weighted 3D IR-UTE-Cones sequence (Figure 4B) were located on the μCT and other UTE images. The high intensity band that lies beneath the superficial layers of cartilage was confirmed to be immediately above the subchondral bone plate on the μCT images (Figure 4A). It shows as high contrast with the $T_1$-weighted UTE sequence but as low contrast with the PD-weighted UTE sequence (Figure 4C). The subchondral bone plate only shows high signal with the selective short $T_2$ UTE imaging sequence (Figure 4D), in which the signal from the superficial, middle and deep layers of uncalcified articular cartilage is suppressed. The deep radial and calcified cartilage (shown on the left-hand side in the red rectangle) was still visible in the short $T_2$ image. These results together suggest that the high intensity band in $T_1$-weighted 3D IR-UTE-Cones imaging mainly comes from the calcified cartilage, with some contribution from the deep radial (uncalcified) layer, but no significant contribution from the subchondral bone plate due to its low proton density (PD).

The OCJ region contrast depends on the choice of $T_I$ as demonstrated by Figure 5. The 3D IR-UTE-Cones images with $T_I$ values from 460 to 600 ms all show high contrast imaging of the OCJ region. $CNR_{OCJ\_SC}$ increased from −14.8 ± 5.2 with a $T_I$ of 220 ms to 20.1 ± 7.4 with a $T_I$ of 540 ms, and then decreased to 15.7 ± 6.6 with a $T_I$ of 800 ms. $CNR_{OCJ\_MF}$ increased from −10.0 ± 3.0 with a $T_I$ of 220 ms to 18.8 ± 6.1 with a $T_I$ of 540 ms, and further increased to 25.0 ± 9.6 with a $T_I$ of 800 ms. An optimal $T_I$ of 540 ms with a maximal $CNR_{OCJ\_SC}$ and good $CNR_{OCJ\_MF}$

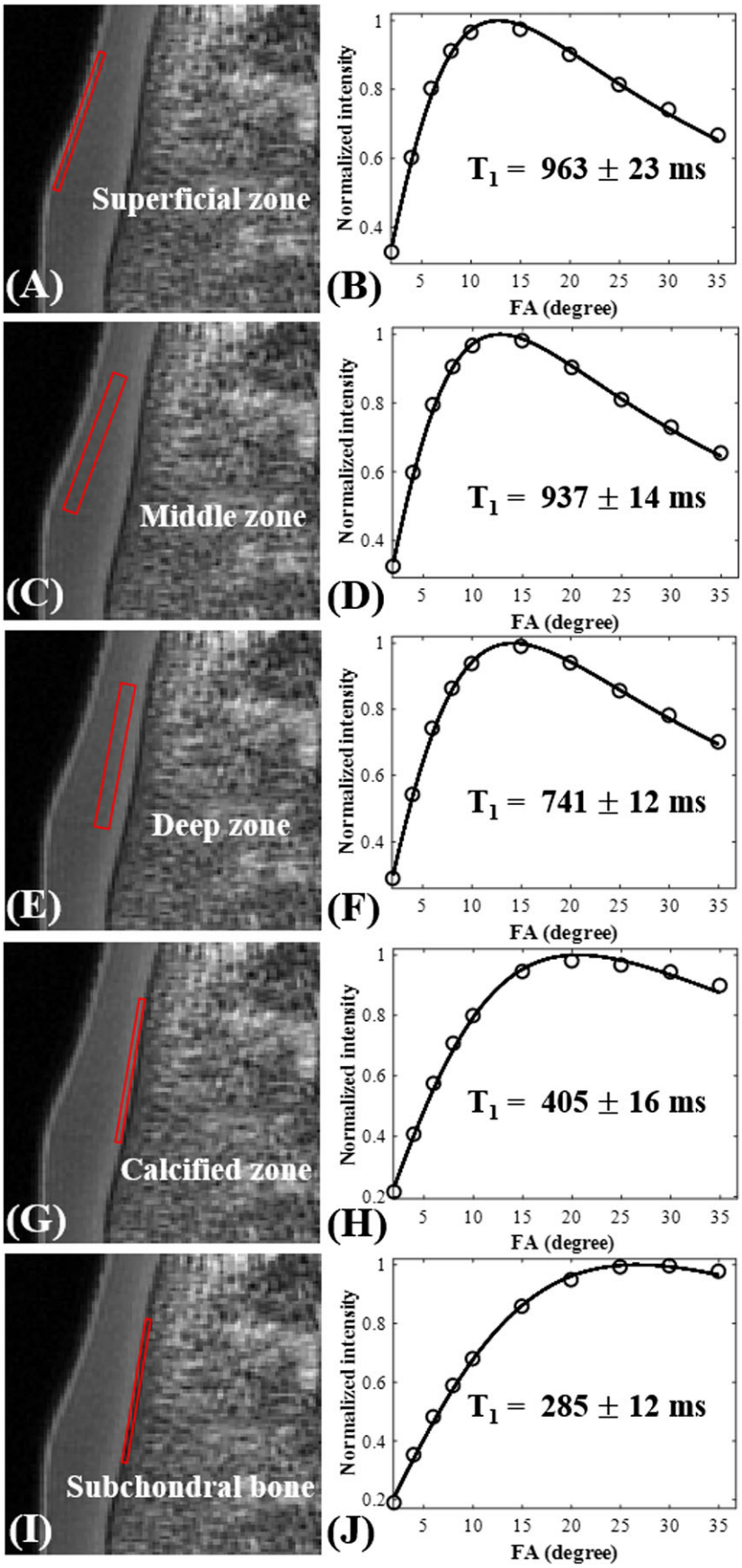


**FIGURE 3** $T_1$ measurements for cartilage and subchondral bone using a 3D UTE-AFI-VFA method for the patellar cartilage sample. A, C, E, G, I, the ROIs (ie red rectangles) from the cartilage surface to the subchondral bone. B, D, F, H, J, the corresponding $T_1$ fitting curves and values

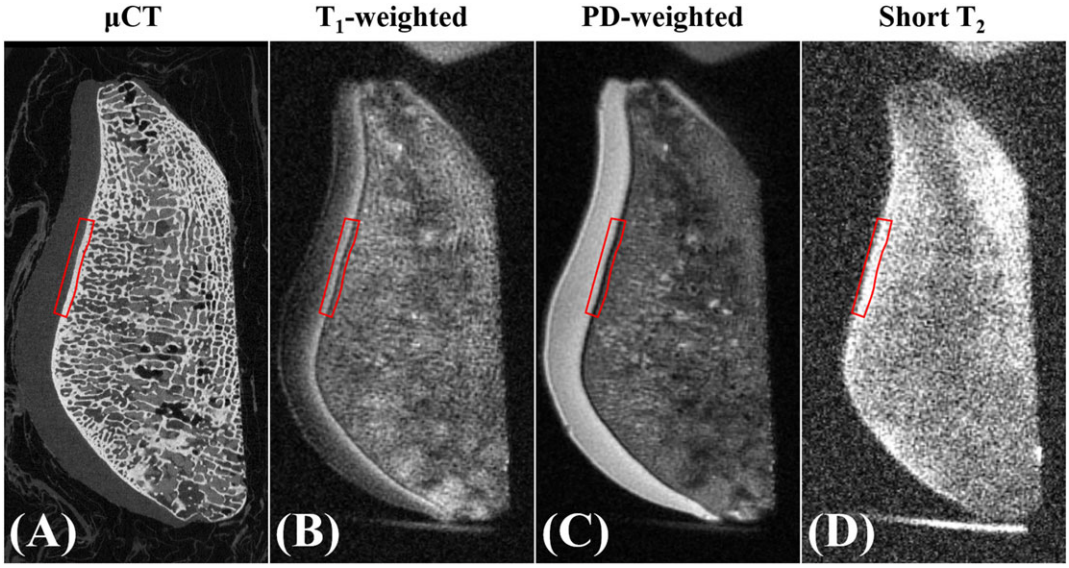


**FIGURE 4** Co-registered high resolution μCT (a) and UTE-MR (B-D) images of the patellar cartilage sample. B, high contrast demonstration of the OCJ region acquired with the $T_1$-weighted IR-UTE-cones sequence ($T_R/T_I$ = 1200/450 ms). C, an approximately PD-weighted image acquired with a much longer $T_I$ using the IR-UTE-cones sequence ($T_R/T_I$ = 1200/1000 ms). D, the pure short $T_2$ components in the cartilage and bone acquired with a very short $T_R$ using the IR-UTE-cones sequence ($T_R/T_I$ = 133/58 ms). The same regions (in red rectangles) including part of the deep layer, calcified layer and subchondral bone were selected for all images

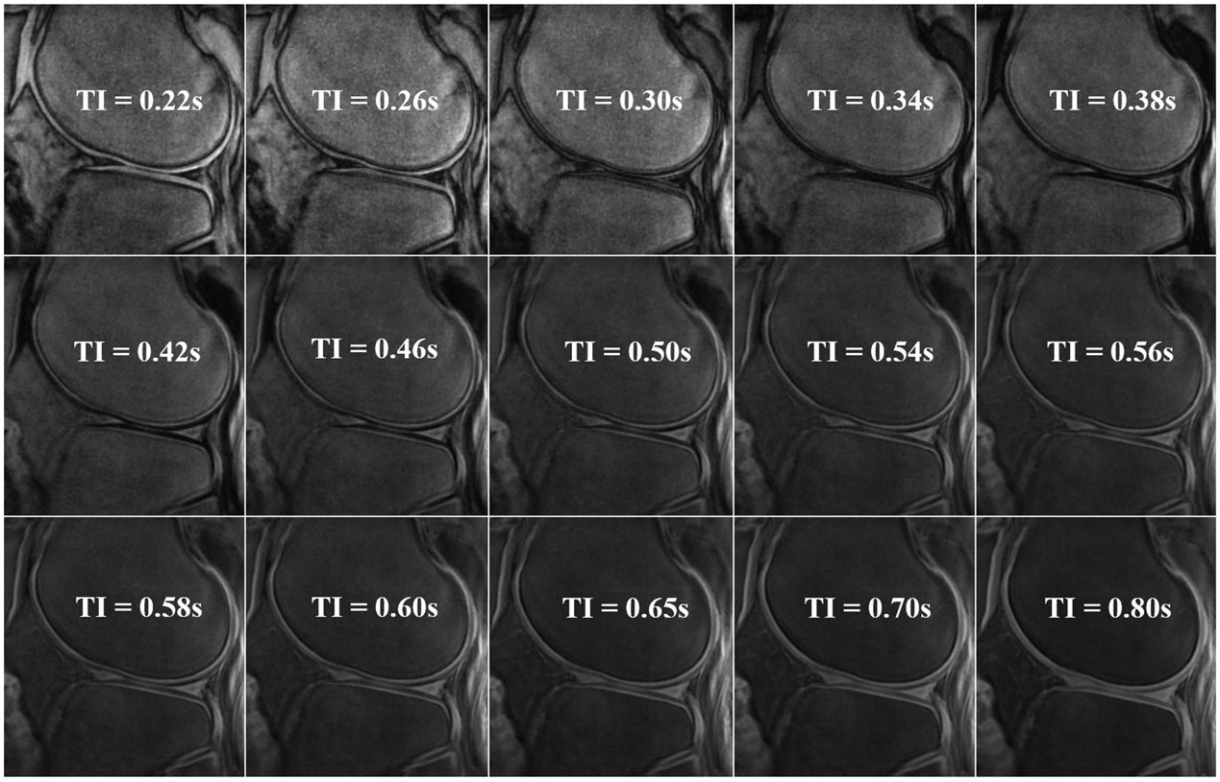


**FIGURE 5** IR-UTE-cones ex vivo knee images (from an 84-year-old male donor) with different $T_I$ values. The $T_R$ is fixed at 1.2 s and $T_I$ varies from 0.22 s to 0.8 s. The contrast of the tissues in the OCJ region varies with the increasing $T_I$

was used for subsequent 3D IR-UTE-Cones imaging of the knee joint specimens. The OCJ contrast was well preserved in the highly accelerated acquisition with an $N_{sp}$ of 21 (Supplementary Figure 2) with the total scan time reduced from 56 min to 10 min. These results support the clinical feasibility of evaluating the OCJ in the whole knee joint in vivo.

The OCJ regions in a normal and abnormal knee joint are displayed in Figures 6 and 7, respectively. The deep layers of articular cartilage, menisci, ligaments and tendons appear with little or no signal with conventional PD- and $T_2$-weighted FSE sequences. The 3D FS-UTE-Cones sequence shows high signal for all the components of articular cartilage, menisci, ligaments and tendons (but not the subchondral bone plate). There is little contrast between the OCJ region and the more superficial layers of articular cartilage, which all show high signal. However, the 3D IR-UTE-Cones sequence shows a well-defined bright band in the patellar, femoral and tibia cartilage of the knee joints. The abnormal knee joint specimen shows morphological changes in the OCJ region, including regions with ill-defined or focal absence of a bright band adjacent to and paralleling the subchondral bone (arrows). These corresponded to abnormal regions on the CT images.

High contrast imaging of the OCJ region in vivo can be obtained within a range of $T_I$ values (ie from 550 to 650 ms), with optimum CNR achieved with a $T_I$ of about 600 ms. Figure 8 shows OCJ region imaging of a normal knee joint. Continuous bright bands can be found in patellar, femoral and tibial cartilages, similar to those observed in the normal knee specimen (Figure 6). $T_1$-weighted 3D IR-UTE-Cones imaging of four OA patients is shown in Figure 9. As with the OA knee specimen, morphological changes were observed in the OCJ region, including ill-defined focal loss and non-visualization of the high intensity band adjacent to the subchondral bone plate (Figure 9). The abnormal OCJ regions shown with the $T_1$-weighted 3D IR-UTE-Cones imaging corresponded well to the abnormal superficial layers seen in the clinical PD- and $T_2$-weighted FSE imaging.

## 4 | DISCUSSION

In this study, we have demonstrated that 3D IR-UTE-Cones sequences can provide high contrast imaging of the OCJ ex vivo and in vivo. The 3D UTE-Cones sequence has a $T_E$ over 100 times shorter than that of conventional clinical sequences, and can directly detect signal from short $T_2$

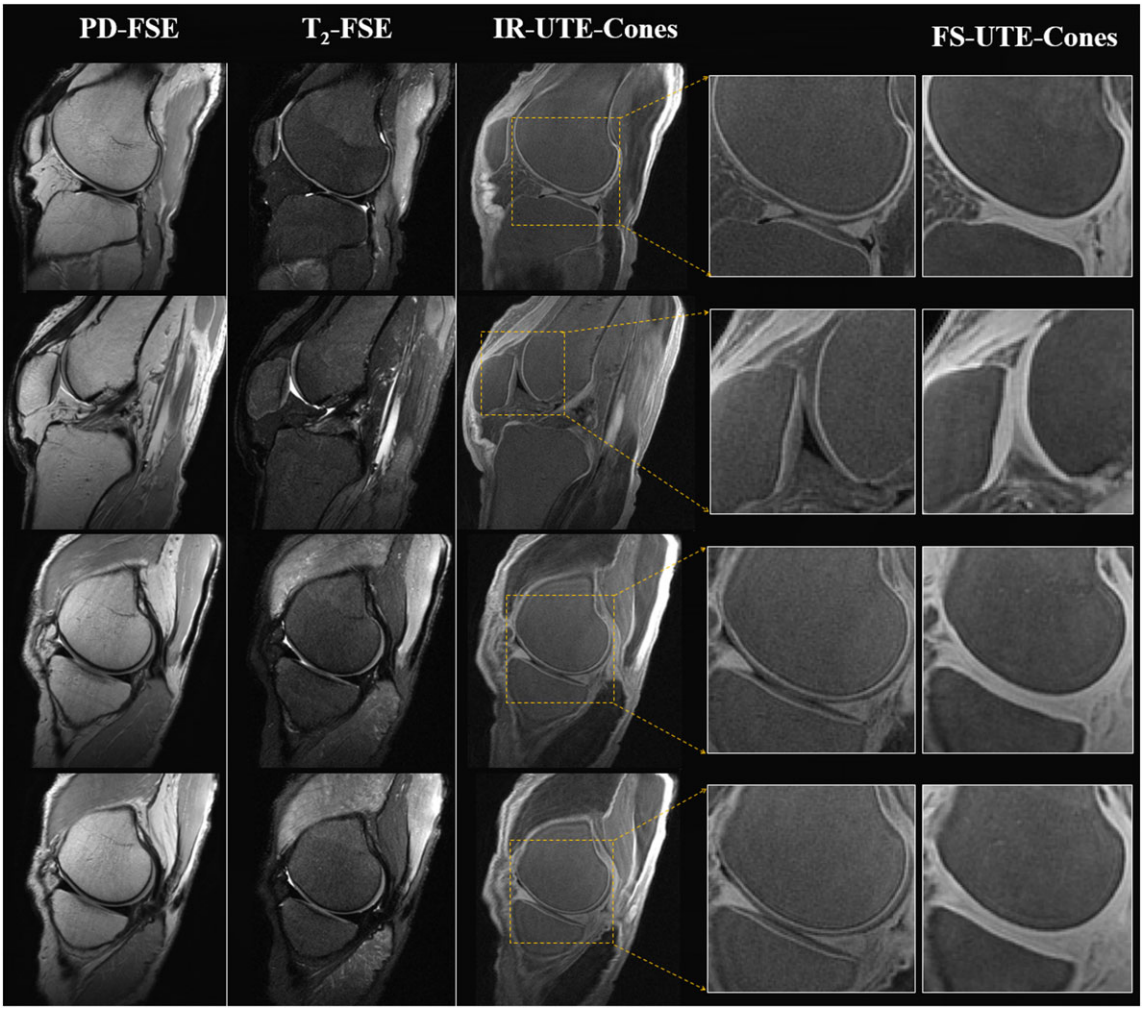


**FIGURE 6** OCJ region imaging of a normal ex vivo knee joint specimen from a 31-year-old donor (male). The clinical images (PD-weighted FSE in first column and $T_2$-weighted FSE in second column) are used for comparison with the $T_1$-weighted IR-UTE-cones images (third column, $T_R/T_I$ = 1200/540 ms). The IR-UTE-cones images show high OCJ contrasts (ie bright band), which can be seen more clearly in the zoomed images. The last column includes the conventional fat-saturated UTE-cones images for comparison. These show signal from both uncalcified and calcified cartilage

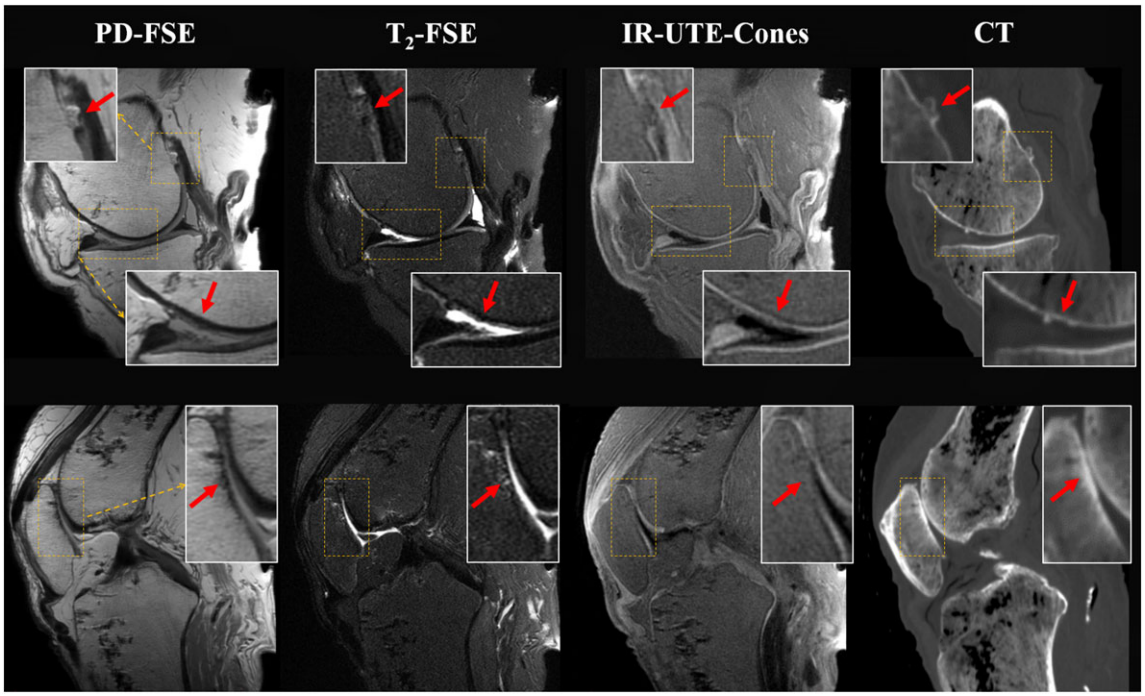


**FIGURE 7** Comparison of CT and MRI of an abnormal ex vivo knee specimen from a 57-year-old donor (male). $T_1$-weighted IR-UTE-cones images show darker and discontinuous regions of calcified cartilage bands, which on CT images correspond to an osteophyte at the posterior-most portion of the medial femoral condyle (top insert), small foci of calcium at the weight-bearing portion of the medial femoral condyle (middle insert) and eburnation at the patella (bottom insert)

tissues or tissue components in the OCJ region, including the calcified cartilage and subchondral bone. The major challenge is the high signal from the surrounding, more superficial layers of articular cartilage and marrow fat. Adiabatic IR preparation pulses provide a very effective method for suppressing signal from longer $T_2$ cartilage, enabling direct demonstration of the OCJ region with high contrast. The much shorter $T_1$ of the OCJ than that of the more superficial layers of articular cartilage further enables high resolution imaging of the OCJ when a highly $T_1$-weighted 3D IR-UTE-Cones sequence is used. Joint fluid with a much longer $T_1$ than either cartilage or marrow is almost completely nulled. The multi-spoke acquisition scheme provides very efficient method of reducing the total scan time without significant compromise in contrast (Supplementary Figure 2), making it clinically feasible to image the OCJ region in vivo.

The signal sources for 3D IR-UTE-Cones imaging of the OCJ region largely comprise the calcified cartilage and part of the deep radial layers of articular cartilage, with little contribution from the subchondral bone plate due to its low PD. The superficial and middle layers as well as part of the radial layer of articular cartilage have relatively long $T_2$ and $T_1$ values, and can be well suppressed by adiabatic inversion pulses. The deep radial cartilage next to the calcified cartilage has much a lower $T_1$ and $T_2$, and is only partially suppressed by the adiabatic inversion pulse. Signal from the deep radial cartilage is lower than that from the calcified cartilage, partly because the calcified cartilage has a shorter $T_2^*$ (thus less inversion and signal attenuation by the adiabatic inversion pulse) and a shorter $T_1$ (thus faster signal recovery after the adiabatic inversion pulse). The subchondral bone plate shows as low signal with $T_1$- and PD-weighted 3D IR-UTE-Cones imaging because of its low PD, which is of the order of 30% water by volume.[25] This is much lower than the approximately 80% water by volume for articular cartilage. The bright band in the $T_1$-weighted IR-UTE-Cones image is much wider than the typical calcified cartilage layer, which may be caused by the short $T_2$ blurring, partial volume effect (relatively thick slice of 2 mm and a curved surface) and contribution from deep radial layers, which also have a short $T_1$.

Imaging of the OCJ region is further complicated by the fact that articular cartilage has two forms of water: free water residing in the organic matrix and water bound to the macromolecules. The existence of bound and free water pools has also been confirmed by cross-relaxation imaging experiments,[26] results from recent MR spectroscopy studies[27] and our own studies.[28] Our prior studies suggest that bound water fraction gradually increases from the articular surface (~15%) to the deep cartilage (~20%). Similar to the calcified cartilage, the bound water magnetizations are largely saturated by the adiabatic inversion pulse because of their short $T_2$ values, recovered during the $T_I$ time, and detected by UTE data acquisition. The spatial distribution of bound water also contributes to a spatial gradient of signal intensity from the superficial cartilage to the calcified cartilage. However, the short $T_2$ signal from the calcified cartilage dominates in $T_1$-weighted 3D IR-UTE-Cones imaging, as shown in Figure 4B.

The bright band region in the $T_1$-weighted IR-UTE-Cones image (eg the left-hand side of the red rectangle in Figure 4B) was largely dark in the μCT image (Figure 4A). This means that there are no significant calcifications in the majority of the bright band. The calcified layer should appear

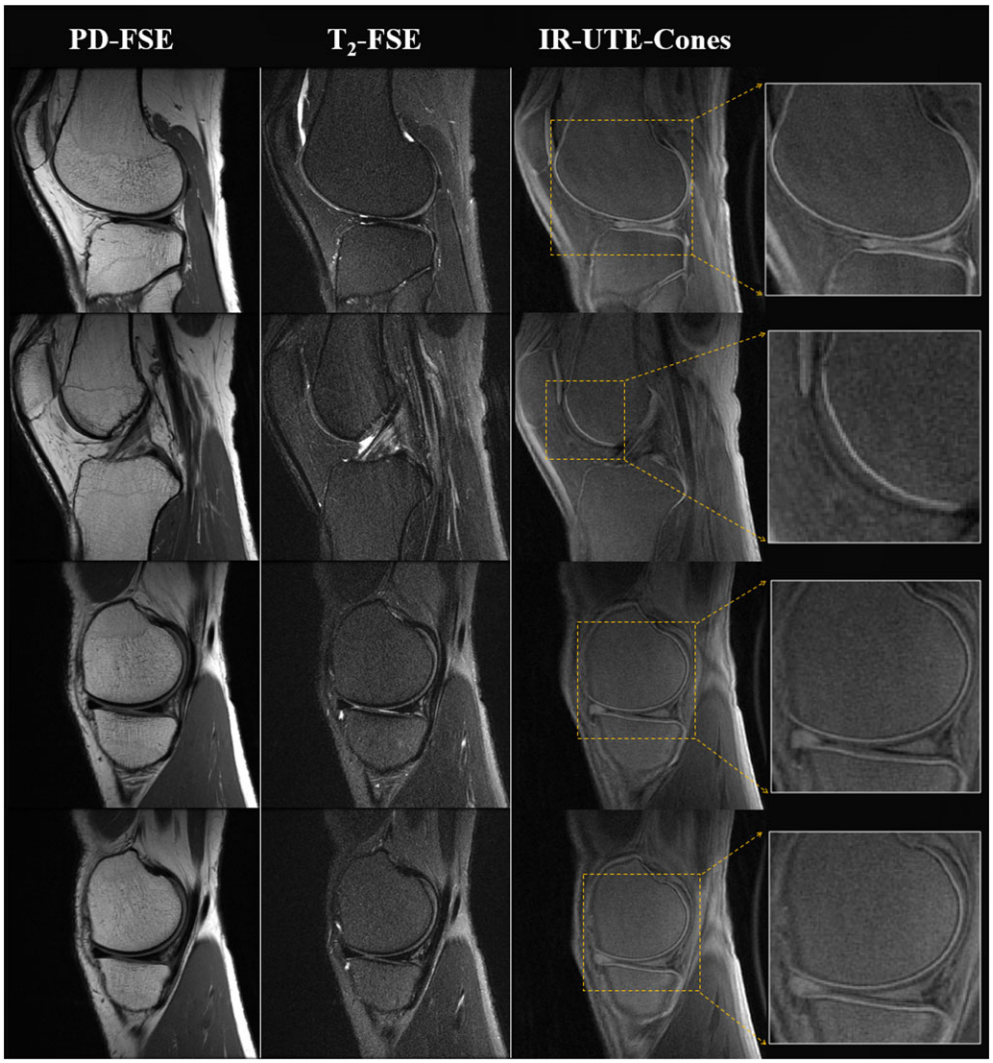


**FIGURE 8** OCJ region imaging of an in vivo knee from a 36-year-old normal volunteer (male). The clinical images (PD-weighted FSE in first column and $T_2$-weighted FSE in second column) are used for comparison with the $T_1$-weighted IR-UTE-cones images (third column, $T_R$/$T_I$ = 1200/600 ms). The IR-UTE-cones images show high OCJ contrasts (ie bright band), which can be seen more clearly in the magnified images

bright in μCT. However, it is very thin and is tightly attached to or overlapped with the subchondral bone. A recent study concluded that μCT with a 2.8 μm isotropic resolution still could not separate calcified cartilage and subchondral bone due to their overlap.[29] Moreover, the IR-UTE-Cones imaging suffered short $T_2$ blurring, off-resonance artifacts and partial volume effect in this study. Thus, it is difficult to get perfect co-registration for MRI and μCT images to isolate the extremely thin calcified layers. A high performance gradient system is necessary for the further verification.

The OCJ serves as a functional barrier between the synovial joint space and subchondral bone marrow, and may play an important role in the pathogenesis of OA.[30-33] Although it is generally thought that the initial changes of OA occur in uncalcified cartilage with degeneration and erosion starting in superficial uncalcified cartilage,[7,8] there are a number of recent studies that are not explained by this model.[4-6,30-32] Calcified cartilage is a highly modified mineralized region with 10–100 times greater stiffness than uncalcified cartilage but an order of magnitude less stiffness than the subchondral bone plate. It functions as a transition zone of intermediate stiffness between uncalcified cartilage and subchondral bone.[30] In OA, calcified cartilage may become reactive and extend to involve adjacent uncalcified cartilage, leading to thinning of the superficial uncalcified layers of cartilage.[31] In a study of OA human femoral heads, the calcified cartilage layer was extremely hypermineralized and twice as hard as neighboring subchondral bone plate.[32] In this situation, it may function as a hard grinding abrasive and accelerate wear rates. Changes in the calcified cartilage can compromise the uncalcified portion and cause it to degenerate.[33,34] The hypermineralized calcified cartilage may have reduced $T_2^*$ and $T_1$ relaxation times; however, its water content may also be reduced (more mineral, less water). Therefore, the 3D IR-UTE signal intensity of hypermineralized calcified cartilage may be higher (if $T_1$ shortening dominates) or lower (if water content reduction dominates) than that of the normal calcified cartilage. In this study, the signal loss of the bright band in the OA patients may be also caused by the degeneration of the cartilage (eg more free water and longer $T_1$). Thus the OCJ region appeared dark in the $T_1$-weighted IR-UTE-Cones sequence.

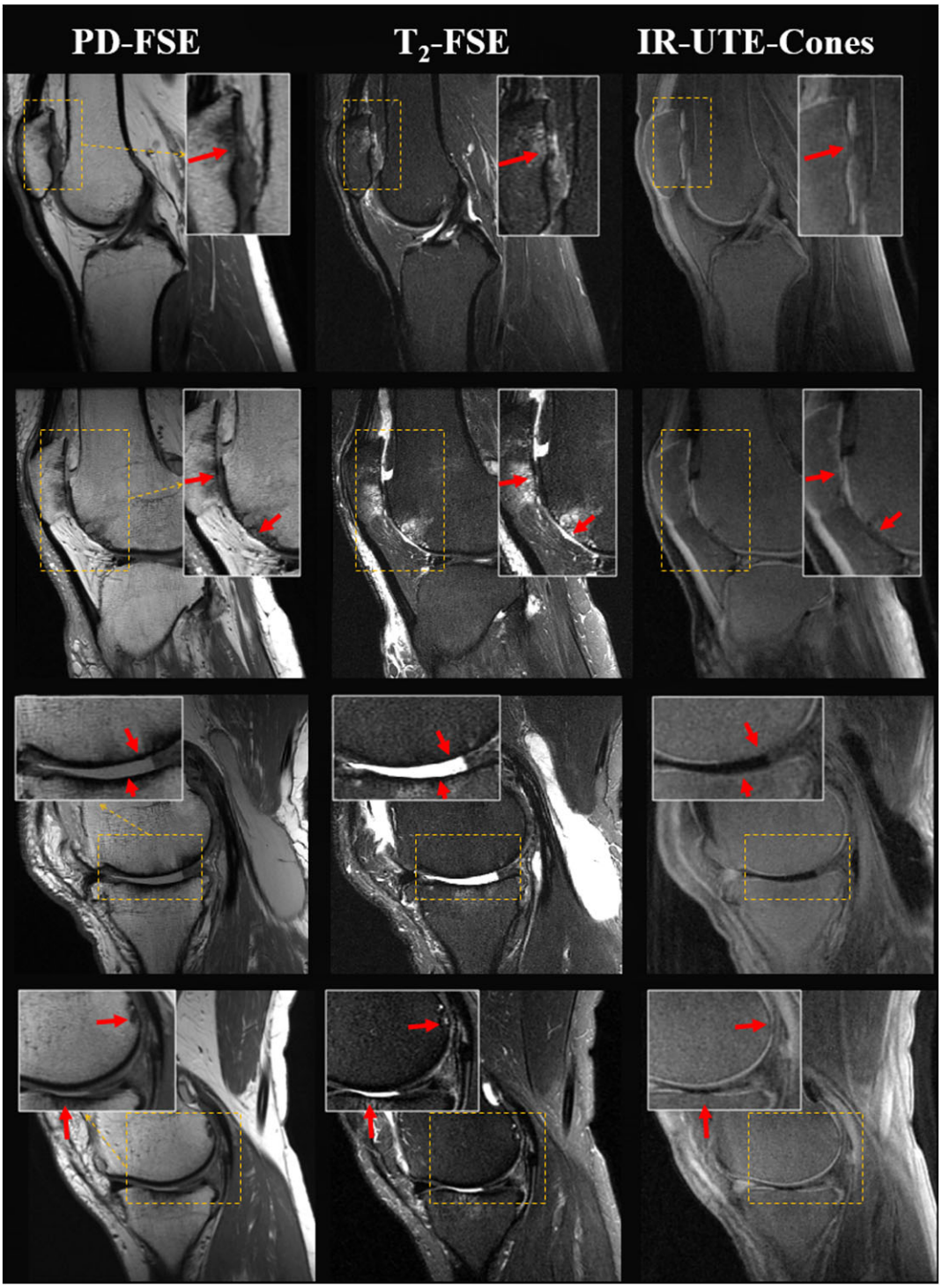


**FIGURE 9** The OCJ imaging of four abnormal in vivo knees from four patients (ages of 54 (female), 49 (male), 54 (male) and 63 (female) years old). The clinical images (PD-weighted FSE in first column and $T_2$-weighted FSE in second column) are used for comparison with the $T_1$-weighted IR-UTE-cones images (third column, $T_R/T_I$ = 1200/600 ms). The arrows show abnormal regions (magnified) on the images with reduction or loss of the high intensity band in the OCJ regions

The OCJ region may play an important role in the initiation and/or progression of OA. MRI of the OCJ region may therefore be of critical importance in elucidating the structural and functional pathogenesis of OA, including features associated with the internal layers of cartilage without loss of superficial layers. Clearly, more research is needed to investigate the morphology of normal versus abnormal deep radial/calcified cartilage (including normal mineralized and hypermineralized calcified cartilage and degeneration of cartilage). Also, quantitative evaluation of the calcified cartilage, including measurement of MR relaxation times ($T_1$, $T_2$, $T_2^*$ and $T_{1\rho}$)[35] and PD, is of high interest and will be investigated in future studies.

There are several limitations of this study. First, histology was not performed to confirm the signal source of the 3D IR-UTE-Cones imaging. However, μCT images supported the view that the high intensity band arises from the deep radial and calcified cartilage without contribution from the subchondral bone. Second, only a small number of knee joint specimens were studied. Abnormalities in the deep radial and calcified cartilage were observed, but without systematic investigation and especially correlation with histology. The 3D IR-UTE-Cones sequence may help with more accurate diagnosis of early OA by exploiting a completely different approach from the conventional MR sequences. The deep radial and calcified cartilage are involved in OA but have never been investigated with clinical MRI. Third, only a small number of healthy volunteers and OA patients were studied. The clinical significance of this technique remains to be further investigated. However, well preserved high intensity bands were observed in the knee joints of all healthy volunteers, while abnormalities in deep radial and calcified cartilage were only depicted in OA patients. These preliminary results clearly demonstrate the clinical potential of the 3D IR-UTE-Cones sequence for evaluating the involvement of deep radial and calcified cartilage in degeneration. Fourth, the scan time of 10 min is still relatively long for clinical scans. Fast acquisition with accelerated techniques such as parallel imaging or compressed sensing may be used in future studies.[36] Fifth, both the PD of the tissues in OCJ region and the distance between the bright bands in femur condyle and tibia may provide us with more information to identify the abnormality related to different OA stages. Other quantitative biomarkers (such as $T_1$, $T_2^*$, $T_2$ and $T_{1\rho}$) may also be included for more comprehensive evaluation. A grading system involving both morphological and quantitative evaluation of the OCJ region remains to be developed.

In conclusion, we have shown that the 3D IR-UTE-Cones sequence can be used to image the OCJ region in vivo. Abnormalities in the OCJ region (mainly the deep radial and calcified cartilage) can be depicted with high spatial resolution and high contrast. This technique could be used for larger scale clinical evaluation of the involvement of the OCJ region in OA, especially in the early stages.

## ACKNOWLEDGEMENTS

The authors acknowledge grant support from GE Healthcare, NIH (1R01 AR062581, 1R01 NS092650 and 1R01 AR068987) and the VA Clinical Science and Rehabilitation Research & Development Services (1I01CX001388 and I01RX002604).

## ORCID

*Ya-Jun Ma* https://orcid.org/0000-0003-0830-9232
*Saeed Jerban* https://orcid.org/0000-0001-6450-2892
*Hyungseok Jang* https://orcid.org/0000-0002-3597-9525
*Jiang Du* https://orcid.org/0000-0002-9203-2450

## REFERENCES

1. Lawrence RC, Felson DT, Helmick CG, et al. Estimates of the prevalence of arthritis and other rheumatic conditions in the United States. Part II. *Arthritis Rheum*. 2008;58(1):26-35.
2. Loeser RF, Goldring SR, Scanzello CR, Goldring MB. Osteoarthritis: a disease of the joint as an organ. *Arthritis Rheum*. 2012;64(6):1697-1707.
3. Mapp PI, Walsh DA. Mechanisms and targets of angiogenesis and nerve growth in osteoarthritis. *Nat Rev Rheumatol*. 2012;8(7):390-398.
4. Walsh DA, McWilliams DF, Turley MJ, et al. Angiogenesis and nerve growth factor at the osteochondral junction in rheumatoid arthritis and osteoarthritis. *Rheumatology*. 2010;49(10):1852-1861.
5. Suri S, Gill SE, Massena de Camin S, Wilson D, McWilliams DF, Walsh DA. Neurovascular invasion at the osteochondral junction and in osteophytes in osteoarthritis. *Ann Rheum Dis*. 2007;66(11):1423-1428.
6. Findlay DM, Atkins GJ. Osteoblast-chondrocyte interactions in osteoarthritis. *Curr Osteoporos Rep*. 2014;12(1):127-134.
7. Choi JA, Gold GE. MR imaging of articular cartilage physiology. *Magn Reson Imaging Clin N Am*. 2011;19(2):249-282.
8. Chang EY, Ma Y, Du J. MR parametric mapping as a biomarker of early joint degeneration. *Sports Health*. 2016;8(5):405-411.
9. Gold GE, Thedens DR, Pauly JM, et al. MR imaging of articular cartilage of the knee: new methods using ultrashort TEs. *Am J Roentgenol*. 1998;170(5):1223-1226.
10. Chang EY, Du J, Chung CB. UTE imaging in the musculoskeletal system. *J Magn Reson Imaging*. 2015;41(4):870-883.
11. Bae WC, Dwek JR, Znamirowski R, et al. Ultrashort echo time MR imaging of osteochondral junction of the knee at 3 T: identification of anatomic structures contributing to signal intensity. *Radiology*. 2010;254(3):837-845.
12. Du J, Takahashi A, Bae WC, Chung CB, Bydder GM. Dual inversion recovery ultrashort echo time (DIR UTE) imaging: creating high contrast for short-$T_2$ species. *Magn Reson Med*. 2010;63:447-455.
13. Du J, Carl M, Bae WC, et al. Dual inversion recovery ultrashort echo time (DIR-UTE) imaging and quantification of the zone of calcified cartilage. *Osteoarthr Cartil*. 2013;21:77-85.
14. Mackay JW, Low SB, Houston GC, Toms AP. Ultrashort TE evaluation of the osteochondral junction *in vivo*: a feasibility study. *Br J Radiol*. 2016;89(1059):20150493.
15. Lu A, Daniel BL, Pauly JM, Pauly KB. Improved slice selection for R2* mapping during cryoablation with eddy current compensation. *J Magn Reson Imaging*. 2008;28:190-198.

16. Lane LB, Bullough PG. Age-related changes in the thickness of the calcified zone and the number of tidemarks in adult human articular cartilage. *J Bone Joint Surg Br*. 1980;62:372-375.
17. Du J, Bydder M, Takahashi AM, Carl M, Chung CB, Bydder GM. Short T2 contrast with three-dimensional ultrashort echo time imaging. *Magn Reson Imaging*. 2011;29:470-482.
18. Van Dyck P, Vanhevel F, Vanhoenacker FM, et al. Morphological MR imaging of the articular cartilage of the knee at 3 T—comparison of standard and novel 3D sequences. *Insights Imaging*. 2015;6(3):285-293.
19. Williams AA, Titchenal MR, Do BH, Guha A, Chu CR. MRI UTE-T2* shows high incidence of cartilage subsurface matrix changes 2 years after ACL reconstruction. *J Orthop Res*. 2018. https://doi.org/10.1002/jor.24110
20. Carl M, Bydder GM, Du J. UTE imaging with simultaneous water and fat signal suppression using a time-efficient multi-spoke inversion recovery pulse sequence. *Magn Reson Med*. 2016;76:577-582.
21. Zanganeh S, Shao H, Bydder GM, Du J. Ultrashort echo time (UTE) imaging of articular cartilage. In: Zia Y, Mornot K, eds. *Biophysics and Biochemistry of Cartilage by NMR and MRI*. (London): Royal Society of Chemistry; 2015 Chapter 11.
22. Larson PE, Conolly SM, Pauly JM, Nishimura DG. Using adiabatic inversion pulses for long-$T_2$ suppression in ultrashort echo time (UTE) imaging. *Magn Reson Med*. 2007;58:952-961.
23. Ma YJ, Lu X, Carl M, et al. Accurate T1 mapping of short T2 tissues using a three-dimensional ultrashort echo time cones actual flip angle-variable TR (3D UTE-cones AFI-VTR) method. *Magn Reson Med*. 2018;80:598-608.
24. Ma YJ, Zhao W, Wan L, et al. Whole knee joint T1 values measured in vivo at 3T by combined 3D ultrashort echo time cones actual flip angle and variable flip angle methods. *Magn Reson Med*. 2018. https://doi.org/10.1002/mrm.27510
25. Manhard MK, Horch RA, Gochberg DF, Nyman JS, Does MD. In vivo quantitative MR imaging of bound and pore water in cortical bone. *Radiology*. 2015;25;277(1):221-229.
26. Stikov N, Keenan KE, Pauly JM, Smith RL, Dougherty RF, Gold GE. Cross-relaxation imaging of human articular cartilage. *Magn Reson Med*. 2011;66:725-734.
27. Reiter DA, Lin PC, Fishbein KW, Spencer RG. Multicomponent $T_2$ relaxation analysis in cartilage. *Magn Reson Med*. 2009;61:803-809.
28. Pauli C, Bae WC, Lee M, et al. Ultrashort echo time (UTE) magnetic resonance imaging of the patella with bi-component analysis: correlation with histopathology and polarized light microscopy. *Radiology*. 2012;264:484-493.
29. Kauppinen S, Karhula SS, Thevenot J, et al. 3D morphometric analysis of calcified cartilage properties using micro-computed tomography. *Osteoarthr Cartil*. 2019;27(1):172-180.
30. Mente PL, Lewis JL. Elastic modulus of calcified cartilage is an order of magnitude less than that of subchondral bone. *J Orthop Res*. 1994;12:637-647.
31. Anderson DD, Brown TD, Radin EL. The influence of basal cartilage calcification on dynamic juxtaarticular stress transmission. *Basal Cartilage Calcification*. 1993;(286):298-307.
32. Ferguson VL, Bushby AJ, Boyde A. Nanomechanical properties and mineral concentration in articular calcified cartilage and subchondral bone. *J Anat*. 2003;203:191-199.
33. Oegema TR, Carpenter RJ, Hofmeister F, Thompson RC. The interaction of the zone of calcified cartilage and subchondral bone in osteoarthritis. *Microsc Res Tech*. 1997;37:324-332.
34. Revell PA, Pirie C, Amir G. Rashad, Walker F. Metabolic activity in the calcified zone of cartilage: observations on tetracycline labeled articular cartilage in human osteoarthritic hips. *Rheumatol Int*. 1990;10:143-147.
35. Ma YJ, Carl M, Shao H, Tadros AS, Chang EY, Du J. Three-dimensional ultrashort echo time cones $T_{1\rho}$ (3D UTE-cones-$T_{1\rho}$) imaging. *NMR Biomed*. 2017;30(6):e3709.
36. Lustig M, Donoho D, Pauly JM. Sparse MRI: the application of compressed sensing for rapid MR imaging. *Magn Reson Med*. 2007;58:1182-1195.

## SUPPORTING INFORMATION

Additional supporting information may be found online in the Supporting Information section at the end of the article.

**How to cite this article:** Ma Y-J, Jerban S, Carl M, et al. Imaging of the region of the osteochondral junction (OCJ) using a 3D adiabatic inversion recovery prepared ultrashort echo time cones (3D IR-UTE-cones) sequence at 3 T. *NMR in Biomedicine*. 2019;e4080. https://doi.org/10.1002/nbm.4080